

Zepto to Attosecond core-level photoemission time delays in homonuclear diatomic molecules and non-dipole effects in the framework of Multiple Scattering theory

Yoshiaki Tamura^{1*}, Kaoru Yamazaki², Kiyoshi Ueda^{3,4} and Keisuke Hatada^{1*}

¹ *Department of Physics, University of Toyama, 3190 Gofuku, 930-8555 Toyama, Japan*

² *Attosecond Science Research Team, Extreme Photonics Research Group, RIKEN Center for Advanced Photonics, RIKEN, 2-1 Hirosawa, Wako, 351-0198 Saitama, Japan.*

³ *Department of Chemistry, Graduate School of Science, Tohoku University, 6-3 Aramaki Aza-Aoba, Aoba-ku, 980-8578 Sendai, Japan and*

⁴ *School Physical Science and Technology, ShanghaiTech University, Shanghai 201210, P. R. China*
(Dated: February 6, 2024)

We report a theoretical study of the angular distribution of core-level photoemission time delay in a molecular frame, which is converting into possible measure with the development of attosecond pulsed lasers and metrology, focusing on homonuclear diatomic molecules. Two-center interference patterns in *gerade* and *ungerade* core-level molecular-frame photoelectron angular distributions (MFPADs) of homonuclear diatomic molecules exhibit symmetry-broken with respect to the direction of light propagation due to the non-dipole (multipole) effect. This non-dipole effect reflects the zeptosecond time difference in the birth of the photoelectron waves at the two absorbing atoms. In this study, we investigate the photoemission time delay due to the non-dipole effect by introducing a theoretical model. We show that in incoherent sums, considering the average of the contributions from the *gerade* and *ungerade* delocalized core states, two-center interference terms cancel each other out in both of the MFPADs and photoemission time delays; however, there remains a residual term exhibiting the non-dipole effect for the photoemission time delays. By expanding the scattering state of photoelectrons with Multiple Scattering theory, we also demonstrate that the scattering effect at the molecular potential plays a crucial role in the descriptions of the photoemission time delays of homonuclear diatomic molecules. Furthermore, we demonstrated that the direct wave contribution does not show angular dependence in the photoemission time delays. We then apply the theoretical model to a nitrogen molecule to show the energy- and angular dependence of the MFPADs and photoemission time delays both analytically and numerically. While the incoherent sums of the MFPADs in a given and opposite direction have the same intensity, the incoherent sums of the photoemission time delays depicts a few hundred zeptosecond difference from numerical calculations by multiple scattering code. Our results reveal that the photoemission time delay is a powerful tool in the probe of attosecond and zeptosecond photoionization dynamics for information missed in the MFPAD. This study will be a basis of theoretical studies of photoionization phenomena in nano systems with many identical atoms, such as large polyatomic molecules and condensed matters to examine their photoemission time delays and non-dipole effects.

I. INTRODUCTION

In this decade, attosecond pulsed lasers have been facilitating experimental exploration of attosecond-scale electron dynamics [1–3]. One of the fundamental questions that the latest attosecond metrology has addressed is to quantify the timescale of photoionization, as highlighted in the 2023 Nobel Prize in Physics [4]. The photoemission time delay reflects atto to zeptosecond (10^{-18} - 10^{-21} sec.) electron dynamics, including its phase, *e.g.* zeptosecond photon-electron interaction [5, 6] and subsequent electron excitation [7–9], attosecond scattering and trapping with surrounding potentials during electron propagation in matter [9–18], and subsequent escape and hole localization [19], and are mostly independent of the slower femtosecond structural dynamics. Photoemission time delay measurements are also expected to provide real-

time information on ultrafast phenomena that have been unobservable until now, as well as attosecond probes on various chemical reaction dynamics.

As proof-of-principle experiments, photoemission time delay in the XUV region has been measured for atoms [7, 10–12, 14, 20–22], molecules [8, 9, 13, 15–18, 23, 24], clusters [19], and condensed phases [25, 26]. The photoemission angle dependence of the molecular photoemission time delay due to anisotropy of molecular potentials has been theoretically predicted [27–33]. A combination of Cold Target Recoil Ion Momentum Spectroscopy with the attosecond pulse trains recently realized the angle-resolved measurement of photoemission time delay in molecular frame [8, 9, 17, 18]. It has also become possible to measure the photoemission time delay of $1s$ core-level electrons by soft X-ray attosecond pulses, and this is expected to be extended to solid and liquid phases.

Many studies have reported the angular dependence of photoelectron emission from the core orbitals of diatomic molecules, providing a solid basis on extension to more complex molecular systems. In molecules with localized core orbitals, such as heteronuclear diatomic

* Authors to whom any corresponding should be addressed
E-mail: hatada@sci.u-toyama.ac.jp,
yoshiakitamura.susa@gmail.com

molecules, core-level Molecular Frame Photoelectron Angular Distribution (MFPAD) shows interference patterns due to multiple scattering in the molecular potential [34]. In contrast, in homonuclear diatomic molecules with non-localized core orbitals, the core-level MFPAD exhibits characteristic oscillation patterns [35–38] related to Cohen-Fano two-center interference [39] in addition to multiple scattering one. The photoemission time delay in such two-center systems has been reported theoretically [27, 28] and experimentally [40], within the dipole approximation.

Recently, a remarkable symmetry breaking with respect to the direction of light propagation on the oscillation pattern due to two-center interference in MFPAD of hydrogen molecules has been experimentally observed with high-precision measurements at high photon energy of light [41]. This symmetry breaking comes from a non-dipole (multipole) effect ignored in the Electric Dipole model and is observed in the region where the photon energy is above ~ 500 eV [42, 43]. Such non-dipole effect can be interpreted as a zeptosecond time difference in the birth of photoemission waves at the two light-absorbing atoms because of the light propagation between the two atoms [44].

The above described non-dipole effects stemming from the equivalent atoms may play a key role in photoelectron angular distributions in various systems to our knowledge; however, such non-dipole effects have not been fully examined. Furthermore, the photoemission time delay may provide additional insights that are not seen by angle-resolved photoelectron spectroscopy, such as the phase information of the non-dipole transition amplitudes as studied for atoms [5, 6]. Homonuclear diatomic molecules are the smallest system with two identical atoms. Theoretical investigations of the non-dipole effect on core-level MFPAD and molecular-frame photoemission time delay in homonuclear diatomic molecules should therefore be a basis for the extension of these nano systems.

In this study, we derive a theoretical model for the core-level photoemission time delay on homonuclear diatomic molecules using the single channel, one-photon, and one-electron ionization from the core-levels of homonuclear diatomic molecules, combined with an approximation beyond Electric Dipole approximation. Moreover, we analytically determine the essential contributions of photoelectron scattering by molecular potentials to the two-center interference and the non-dipole effect in the photoemission time delay and derive analytical expressions. We then compare the calculations based on the derived analytical formula and the numerical calculations for nitrogen molecule. These exercises reveal new insights into non-dipole effects in core-level photoemission from two equivalent atoms.

In brief, when the molecule is aligned along the light propagation, our model reproduces the backward-forward tilt of the oscillation pattern of the two-center interference observed in the MFPAD both for *grade* and

ungerade core states as previously reported [41, 44]. The corresponding photoemission time delay goes to the extreme value at emission angles where the MFPAD goes to zero, exhibiting forward and backward asymmetry. Most importantly, if we take an incoherent sum of the *gerade* and *ungerade* core state, as in most of the experiments, then the forward and backward asymmetry in the MFPAD along the direction of light propagation disappears, whereas the asymmetry in the photoemission time delay due to non-dipole effects survives. Our analysis evidences that the non-dipole photoemission time delay includes the information about a zeptosecond-order time delay related to the electron dynamics immediately after light irradiation, which cannot be extracted from MFPADs.

II. THEORY

In this study, we employ the following expression for the photoionization amplitude based on a one-photon and one-electron picture and a single-channel model within the first-order perturbation theory: in length gauge [45]:

$$\langle \psi^-(\mathbf{k}) | e^{i\boldsymbol{\kappa}\cdot\mathbf{r}} \hat{\boldsymbol{\epsilon}} \cdot \mathbf{r} | \phi_{\text{ini}} \rangle. \quad (1)$$

Here, we use atomic units for length and Rydberg units for energies ($2m/\hbar^2 \rightarrow 1$, thus $k^2 = E$) throughout the paper without further notice. $|\psi^-(\mathbf{k})\rangle$ is a photoelectron continuum state with incoming boundary condition and the momentum vector \mathbf{k} and $|\phi_{\text{ini}}\rangle$ is an initial state. $\hat{\boldsymbol{\epsilon}}$ and $\boldsymbol{\kappa}$ are polarization and momentum vector of incoming light, respectively.

A. Treatment of initial orbitals and continuum states of homonuclear diatomic molecules

In homonuclear diatomic molecules, we need to consider the effect of *gerade* and *ungerade* states for the initial state [46] to evaluate their photoelectron time delay unlike heteronuclear diatomic molecules [47]. We represent them by a linear combination of core wave functions, which are spherically symmetric and are confined in concentric atomic spheres with atoms 1 and 2, respectively, with a radius b and not overlapping each other. (Fig. 1):

$$\phi^{g/u}(\mathbf{r}) = \frac{1}{\sqrt{2}} \left[\Theta(r_1 - b) \phi_{1,L_c}(r_1) \pm \Theta(r_2 - b) \phi_{2,L_c}(r_2) \right], \quad (2)$$

where the subscript g/u denotes *gerade/ungerade* state. \mathbf{r} is a position vector from the origin O where is the center of gravity of the molecule. $r_i = |\mathbf{r}_i|$ is a norm of a position vector from the center of atom i , $\Theta(x)$ is a step function if $x \leq 0$ then $\Theta(x) = 1$ else $\Theta(x) = 0$. $\phi_{i,L_c}(r_i)$ is a core wave function of atom i with angular momentum quantum number $L_c \equiv (l_c, m_c) = (0, 0)$.

The continuum wavefunction of photoelectron, ψ^- , is partitioned into four regions in space as [48],

$$\begin{aligned} \psi^-(\mathbf{k}, \mathbf{r}) = & \sum_{j=1}^2 \Theta(r_j - b) \psi_j^-(\mathbf{k}, \mathbf{r}_j) \\ & + \prod_{j=1}^2 [1 - \Theta(r_j - b)] \Theta(r - b_{os}) \psi_{\text{II}}^-(\mathbf{k}, \mathbf{r}) \\ & + [1 - \Theta(r - b_{os})] \psi_{\text{III}}^-(\mathbf{k}, \mathbf{r}), \end{aligned} \quad (3)$$

where ψ_j^- , ψ_{II}^- and ψ_{III}^- are wavefunctions in regions I_j, II and III, respectively. The region I_j is inside the atomic sphere *j*, and the region II is the interstitial space inside the outer sphere that has a radius b_{os} and is centered at the origin O, and the region III is outside the outersphere. (See Fig. 1)

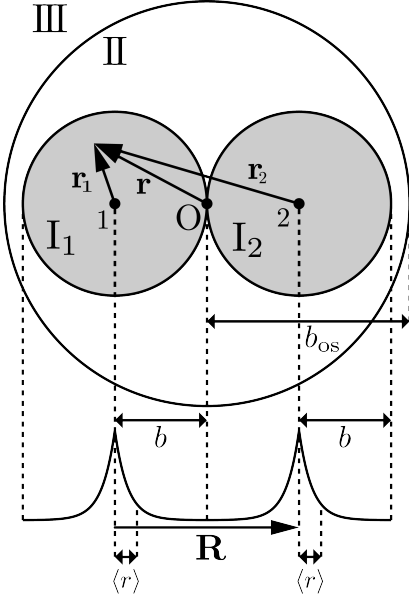


FIG. 1. Partitioning of the molecular space for homonuclear diatomic molecules by atomic spheres 1 and 2 (grey color). They are concentric with atoms (regions I₁ and I₂), and an outer sphere is centered at the origin O, where is the center of gravity of the molecule. We defined the interstitial space in the outer sphere to be region II and the outside of region II to be region III. Here, b is a radius of regions I₁ and I₂, b_{os} is that of region II. \mathbf{r} , \mathbf{r}_1 and \mathbf{r}_2 are position vectors from O, sites 1, and 2, respectively. \mathbf{R} is the vector from the site 1 to 2, and defines molecular axis. We also demonstrated a schematic of the wave function of the *gerade* state within a linear combination of the *1s* hydrogenic atomic orbitals with atomic number $Z = 7$ to explain that the core orbital is well localized for the bond length R . The mean radius of the localized core orbital $\langle r \rangle$ is sufficiently smaller than R .

By substituting Eqs. (2) and (3) into Eq. (1) of the

photoionization amplitude, we get the following equation:

$$\begin{aligned} & \langle \psi^-(\mathbf{k}) | e^{i\boldsymbol{\kappa} \cdot \mathbf{r}} \hat{\boldsymbol{\epsilon}} \cdot \mathbf{r} | \phi^{g/u} \rangle \\ & = \frac{1}{\sqrt{2}} \int_{V_1} d\mathbf{r} \psi_1^{-*}(\mathbf{k}, \mathbf{r}_1) e^{i\boldsymbol{\kappa} \cdot \mathbf{r}} \hat{\boldsymbol{\epsilon}} \cdot \mathbf{r} \phi_{1,L_c}(r_1) \\ & \pm \frac{1}{\sqrt{2}} \int_{V_2} d\mathbf{r} \psi_2^{-*}(\mathbf{k}, \mathbf{r}_2) e^{i\boldsymbol{\kappa} \cdot \mathbf{r}} \hat{\boldsymbol{\epsilon}} \cdot \mathbf{r} \phi_{2,L_c}(r_2), \end{aligned} \quad (4)$$

where the volume integrals, $\int_{V_i} d\mathbf{r}$, are done in the spherical region of site *i* with radius b_i . The first and second terms on the right-hand side are photoionization amplitudes describing the excitation of electrons from the core orbital of atom 1 and 2 to the scattering states in the corresponding regions, respectively.

B. Beyond Electric Dipole approximation describing interatomic light propagation in homonuclear diatomic molecules

Previous studies by Grundmann *et al.* and Iwanov *et al.* have reported that the multipole effect related to light propagation between two atoms plays a crucial role in homonuclear diatomic molecules. [41, 44] To verify this, we separate the light operators, $\exp(i\boldsymbol{\kappa} \cdot \mathbf{r}) \hat{\boldsymbol{\epsilon}} \cdot \mathbf{r}$, in Eq. (4), inducing multipoles into contributions inside and between the atoms. We subsequently shift the origin of the integrals to the center at each site *i*, and then we obtain the following equation:

$$\begin{aligned} & \langle \psi^-(\mathbf{k}) | e^{i\boldsymbol{\kappa} \cdot \mathbf{r}} \hat{\boldsymbol{\epsilon}} \cdot \mathbf{r} | \phi^{g/u} \rangle \\ & = \frac{1}{\sqrt{2}} e^{i\boldsymbol{\kappa} \cdot \mathbf{R}_{1O}} \int_{V_1} d\mathbf{r}_1 \psi_1^{-*}(\mathbf{k}, \mathbf{r}_1) e^{i\boldsymbol{\kappa} \cdot \mathbf{r}_1} \hat{\boldsymbol{\epsilon}} \cdot \mathbf{r}_1 \phi_{1,L_c}(r_1) \\ & + \frac{1}{\sqrt{2}} e^{i\boldsymbol{\kappa} \cdot \mathbf{R}_{1O}} \hat{\boldsymbol{\epsilon}} \cdot \mathbf{R}_{1O} \int_{V_1} d\mathbf{r}_1 \psi_1^{-*}(\mathbf{k}, \mathbf{r}_1) e^{i\boldsymbol{\kappa} \cdot \mathbf{r}_1} \phi_{1,L_c}(r_1) \\ & \pm \frac{1}{\sqrt{2}} e^{i\boldsymbol{\kappa} \cdot \mathbf{R}_{2O}} \int_{V_2} d\mathbf{r}_2 \psi_2^{-*}(\mathbf{k}, \mathbf{r}_2) e^{i\boldsymbol{\kappa} \cdot \mathbf{r}_2} \hat{\boldsymbol{\epsilon}} \cdot \mathbf{r}_2 \phi_{2,L_c}(r_2) \\ & \pm \frac{1}{\sqrt{2}} e^{i\boldsymbol{\kappa} \cdot \mathbf{R}_{2O}} \hat{\boldsymbol{\epsilon}} \cdot \mathbf{R}_{2O} \int_{V_2} d\mathbf{r}_2 \psi_2^{-*}(\mathbf{k}, \mathbf{r}_2) e^{i\boldsymbol{\kappa} \cdot \mathbf{r}_2} \phi_{2,L_c}(r_2) \end{aligned} \quad (5)$$

$$\begin{aligned} & \xrightarrow{\text{E1' approximation } (e^{i\boldsymbol{\kappa} \cdot \mathbf{r}_1}, e^{i\boldsymbol{\kappa} \cdot \mathbf{r}_2} \rightarrow 1)} \\ & \frac{1}{\sqrt{2}} \left(e^{-i\boldsymbol{\kappa} \cdot \frac{\mathbf{R}}{2}} A_1(E1; \mathbf{k}, \hat{\boldsymbol{\epsilon}}) \pm e^{i\boldsymbol{\kappa} \cdot \frac{\mathbf{R}}{2}} A_2(E1; \mathbf{k}, \hat{\boldsymbol{\epsilon}}) \right) \\ & \equiv A^{g/u}(E1'; \mathbf{k}, \hat{\boldsymbol{\epsilon}}, \boldsymbol{\kappa}), \end{aligned} \quad (6)$$

where

$$A_i(E1; \mathbf{k}, \hat{\boldsymbol{\epsilon}}) \equiv \int_{V_i} d\mathbf{r}_i \psi_i^{-*}(\mathbf{k}, \mathbf{r}_i) \hat{\boldsymbol{\epsilon}} \cdot \mathbf{r}_i \phi_{i,L_c}(r_i) \quad (7)$$

is the photoionization amplitude, which describes the Electric Dipole (E1) transition from the core orbital of atom *i*. We used the relation $\mathbf{r} = \mathbf{r}_i + \mathbf{R}_{iO}$, where \mathbf{R}_{iO} is a position vector from the origin O to the center position of atom *i*, hence $\mathbf{R}_{1O} = -\mathbf{R}/2$

and $\mathbf{R}_{2O} = \mathbf{R}/2$. (See Fig. 1) In the last step in Eq. (6), we applied $E1$ approximation only for the transitions inside atoms so that we can effectively incorporate the phase difference in light propagation between two atoms, hereinafter we call it $E1'$ approximation. After applying $E1'$ approximation, we used orthogonality between initial and final electronic wave function [49]

$$\int_{V_i} d\mathbf{r}_i \psi_i^{-*}(\mathbf{k}, \mathbf{r}_i) \phi_{i,L_c}(\mathbf{r}_i) \sim \langle \psi_i^-(\mathbf{k}) | \phi_{i,L_c} \rangle \sim 0. \quad (8)$$

We estimate the validity of $E1'$ approximation using the hydrogen-like atom model. In this model, the expectation value of the radius of $1s$ core orbital is $\langle r \rangle = 3/(2Z)$ a.u. where Z is the atomic number. The $\langle r \rangle$ for nitrogen atom ($Z = 7$) is expected to be $\langle r \rangle = 0.21428$ a.u.. In this case, $E1$ approximation inside the integral works well, and the non-dipole effect inside the atom [5, 6, 50] may be ignored because the maximum absolute value for quadrupole term is calculated to be $\kappa \langle r \rangle \sim 0.074796 \ll 1$ in multipole expansion of $\exp(i\boldsymbol{\kappa} \cdot \mathbf{r}) \sim 1 + i\boldsymbol{\kappa} \cdot \mathbf{r} + \dots$ at photoelectron energy of 900 eV. Conversely, the factor $\exp(i\boldsymbol{\kappa} \cdot \mathbf{R})$ plays an important role of the non-dipole effect on photoemission time delay for nitrogen molecules because its bond length $R = 2.0742$ a.u. and $\kappa R \sim 0.72400$. Notably, the phase difference of the prefactors between A_1 and A_2 is responsible for the non-dipole effect in the photoemission time delay as discussed later in this section.

Applying the above model, the MFPAD from *gerade* and *ungerade* states are reduced as follows:

$$\begin{aligned} I^{g/u}(\mathbf{k}, \hat{\boldsymbol{\epsilon}}, \boldsymbol{\kappa}) &\equiv 8\pi^2 c\kappa \left| \langle \psi^-(\mathbf{k}) | e^{i\boldsymbol{\kappa} \cdot \mathbf{r}} \hat{\boldsymbol{\epsilon}} \cdot \mathbf{r} | \phi^{g/u} \rangle \right|^2 \\ &\xrightarrow{\text{E1' approximation}} 8\pi^2 c\kappa \left| A^{g/u}(E1'; \mathbf{k}, \hat{\boldsymbol{\epsilon}}, \boldsymbol{\kappa}) \right|^2 \\ &\equiv I^{g/u}(E1'; \mathbf{k}, \hat{\boldsymbol{\epsilon}}, \boldsymbol{\kappa}), \quad (9) \end{aligned}$$

where

$$\begin{aligned} I^{g/u}(E1'; \mathbf{k}, \hat{\boldsymbol{\epsilon}}, \boldsymbol{\kappa}) &= \frac{1}{2} I_1(E1; \mathbf{k}, \hat{\boldsymbol{\epsilon}}) + \frac{1}{2} I_2(E1; \mathbf{k}, \hat{\boldsymbol{\epsilon}}) \\ &\pm 8\pi^2 c\kappa \operatorname{Re} \left\{ e^{i\boldsymbol{\kappa} \cdot \mathbf{R}} A_1^*(E1; \mathbf{k}, \hat{\boldsymbol{\epsilon}}) A_2(E1; \mathbf{k}, \hat{\boldsymbol{\epsilon}}) \right\} \quad (10) \end{aligned}$$

and

$$I_i(E1; \mathbf{k}, \hat{\boldsymbol{\epsilon}}) \equiv 8\pi^2 c\kappa |A_i(E1; \mathbf{k}, \hat{\boldsymbol{\epsilon}})|^2 \quad (11)$$

is a MFPAD from a core orbital $\phi_{L_c}^i$ localized in the atom i of homonuclear diatomic molecules. The third term in Eq. (10) describes two-center interference phenomenon.

The photoemission time delays from *gerade* and *ungerade* states are given in the following forms:

$$\begin{aligned} t^{g/u}(\mathbf{k}, \hat{\boldsymbol{\epsilon}}, \boldsymbol{\kappa}) &\equiv \frac{d}{dE_{\mathbf{k}}} \arg \left\{ \langle \psi^-(\mathbf{k}) | e^{i\boldsymbol{\kappa} \cdot \mathbf{r}} \hat{\boldsymbol{\epsilon}} \cdot \mathbf{r} | \phi^{g/u} \rangle \right\} \\ &\xrightarrow{\text{E1' approximation}} \frac{d}{dE_{\mathbf{k}}} \arg \left\{ A^{g/u}(E1'; \mathbf{k}, \hat{\boldsymbol{\epsilon}}, \boldsymbol{\kappa}) \right\} \\ &\equiv t^{g/u}(E1'; \mathbf{k}, \hat{\boldsymbol{\epsilon}}, \boldsymbol{\kappa}). \quad (12) \end{aligned}$$

Using the chain rule of differentiation, we can separate the energy derivative into two terms:

$$\frac{d}{dE_{\mathbf{k}}} = \frac{dk}{dE_{\mathbf{k}}} \frac{\partial}{\partial k} + \frac{d\kappa}{dE_{\mathbf{k}}} \frac{\partial}{\partial \kappa} = \frac{1}{v_g} \frac{\partial}{\partial k} + \frac{1}{c} \frac{\partial}{\partial \kappa}, \quad (13)$$

where $E_{\mathbf{k}} = |\mathbf{k}|^2$ is photoelectron energy, $v_g = dE_{\mathbf{k}}/dk = 2k$ is the group velocity of a free electron wave packet with momentum $k = |\mathbf{k}|$. From a relation $\kappa = |\boldsymbol{\kappa}| = (E_{\mathbf{k}} + I_p)/c$, where I_p is the ionization energy and c is velocity of light, we obtain $d\kappa/dE_{\mathbf{k}} = 1/c$.

The photoemission time delay can be separated by applying Eq. (13) :

$$t^{g/u}(E1'; \mathbf{k}, \hat{\boldsymbol{\epsilon}}, \boldsymbol{\kappa}) = t_{\partial k}^{g/u}(E1'; \mathbf{k}, \hat{\boldsymbol{\epsilon}}, \boldsymbol{\kappa}) + t_{\partial \kappa}^{g/u}(E1'; \mathbf{k}, \hat{\boldsymbol{\epsilon}}, \boldsymbol{\kappa}), \quad (14)$$

where

$$\begin{aligned} t_{\partial k}^{g/u}(E1'; \mathbf{k}, \hat{\boldsymbol{\epsilon}}, \boldsymbol{\kappa}) &\equiv \frac{1}{v_g} \frac{\partial}{\partial k} \arg \left\{ A^{g/u}(E1'; \mathbf{k}, \hat{\boldsymbol{\epsilon}}, \boldsymbol{\kappa}) \right\} \\ &= \left(I^{g/u}(E1'; \mathbf{k}, \hat{\boldsymbol{\epsilon}}, \boldsymbol{\kappa}) \right)^{-1} \left[I_1(E1; \mathbf{k}, \hat{\boldsymbol{\epsilon}}) t_1(E1; \mathbf{k}, \hat{\boldsymbol{\epsilon}}) \right. \\ &\quad \left. + I_2(E1; \mathbf{k}, \hat{\boldsymbol{\epsilon}}) t_2(E1; \mathbf{k}, \hat{\boldsymbol{\epsilon}}) \right. \\ &\quad \left. \pm \operatorname{Im} \left\{ e^{i\boldsymbol{\kappa} \cdot \mathbf{R}} A_1^*(E1; \mathbf{k}, \hat{\boldsymbol{\epsilon}}) \frac{1}{v_g} \frac{\partial}{\partial k} A_2(E1; \mathbf{k}, \hat{\boldsymbol{\epsilon}}) \right. \right. \\ &\quad \left. \left. + e^{-i\boldsymbol{\kappa} \cdot \mathbf{R}} A_2^*(E1; \mathbf{k}, \hat{\boldsymbol{\epsilon}}) \frac{1}{v_g} \frac{\partial}{\partial k} A_1(E1; \mathbf{k}, \hat{\boldsymbol{\epsilon}}) \right\} \right], \quad (15) \end{aligned}$$

$$\begin{aligned} t_{\partial \kappa}^{g/u}(E1'; \mathbf{k}, \hat{\boldsymbol{\epsilon}}, \boldsymbol{\kappa}) &\equiv \frac{1}{c} \frac{\partial}{\partial \kappa} \arg \left\{ A^{g/u}(E1'; \mathbf{k}, \hat{\boldsymbol{\epsilon}}, \boldsymbol{\kappa}) \right\} \\ &= \frac{1}{c} \frac{R}{2} \hat{\boldsymbol{\kappa}} \cdot \hat{\mathbf{R}} \frac{I_2(E1; \mathbf{k}, \hat{\boldsymbol{\epsilon}}) - I_1(E1; \mathbf{k}, \hat{\boldsymbol{\epsilon}})}{2 I^{g/u}(E1'; \mathbf{k}, \hat{\boldsymbol{\epsilon}}, \boldsymbol{\kappa})} \quad (16) \end{aligned}$$

and

$$t_i(E1; \mathbf{k}, \hat{\boldsymbol{\epsilon}}) \equiv \frac{d}{dE_{\mathbf{k}}} \arg \{ A_i(E1; \mathbf{k}, \hat{\boldsymbol{\epsilon}}) \}. \quad (17)$$

Where $t_{\partial k}^{g/u}$ is the photoemission time delay resulting from the k -partial derivative in Eq. (13). The curly bracket in Eq. (15) is responsible for two-center interference phenomenon specific to the photoemission time delay. On the other hand, the first and second terms in Eq. (15) are characterized by t_i which represents a photoemission time delay from a core orbital ϕ_{i,L_c} localized in an atom i of the homonuclear diatomic molecules. More details about t_i are found in reference [47]. $t_{\partial \kappa}^{g/u}$ is the photoemission time delay correspond to the κ -partial derivative in Eq. (13). The factor $(R/2c) \hat{\boldsymbol{\kappa}} \cdot \hat{\mathbf{R}}$ comes from κ -partial derivative of the factor $\exp(\pm i\boldsymbol{\kappa} \cdot \mathbf{R}/2)$, where $R/c \sim 366.12$ zepto sec. is the traveling time for light propagation between atoms. Because both $t_{\partial k}^{g/u}$ and $t_{\partial \kappa}^{g/u}$ are divided by $I^{g/u}$, they exhibit the particular behavior of two-center interference phenomenon specific to MFPAD.

C. Incoherent sums of MFPAD and photoemission time delay for *gerade* and *ungerade* core initial states

In most experiments, it is technically difficult to distinguish photoelectrons from *gerade* and *ungerade* core states as the energy splitting between those states is of the sub-eV order (e.g. 97 meV for nitrogen molecules [51]). This leads to the measurement of the related quantities in the incoherent sums of the *gerade* and *ungerade* states. We can naturally define the incoherent sums of MFPAD, $\langle I \rangle_{\text{IC}}$, and the photoemission time delay, $\langle t \rangle_{\text{IC}}$ as:

$$\langle I \rangle_{\text{IC}} \equiv \frac{1}{2} (I^g + I^u), \quad (18)$$

$$\langle t \rangle_{\text{IC}} \equiv \frac{I^g t^g + I^u t^u}{I^g + I^u}. \quad (19)$$

For the models described in Eqs. (9) and (12), the corresponding incoherent sums for the photoemission time delays are written as follows:

$$\langle I(E1'; \mathbf{k}, \hat{\epsilon}) \rangle_{\text{IC}} = \frac{1}{2} (I_1(E1; \mathbf{k}, \hat{\epsilon}) + I_2(E1; \mathbf{k}, \hat{\epsilon})), \quad (20)$$

$$\begin{aligned} \langle t_{\partial k}(E1'; \mathbf{k}, \hat{\epsilon}) \rangle_{\text{IC}} \\ = \frac{I_1(E1; \mathbf{k}, \hat{\epsilon}) t_1(E1; \mathbf{k}, \hat{\epsilon}) + I_2(E1; \mathbf{k}, \hat{\epsilon}) t_2(E1; \mathbf{k}, \hat{\epsilon})}{2 \langle I(E1'; \mathbf{k}, \hat{\epsilon}) \rangle_{\text{IC}}}, \end{aligned} \quad (21)$$

$$\langle t_{\partial \kappa}(E1'; \mathbf{k}, \hat{\epsilon}, \boldsymbol{\kappa}) \rangle_{\text{IC}} = \frac{R}{2c} \hat{\boldsymbol{\kappa}} \cdot \hat{\mathbf{R}} \frac{I_2(E1; \mathbf{k}, \hat{\epsilon}) - I_1(E1; \mathbf{k}, \hat{\epsilon})}{2 \langle I(E1'; \mathbf{k}, \hat{\epsilon}) \rangle_{\text{IC}}}. \quad (22)$$

$\langle I(E1'; \mathbf{k}, \hat{\epsilon}) \rangle_{\text{IC}}$ and $\langle t_{\partial k}(E1'; \mathbf{k}, \hat{\epsilon}) \rangle_{\text{IC}}$ are independent from the light momentum $\boldsymbol{\kappa}$, because $\boldsymbol{\kappa}$ -dependent terms (the third terms in Eqs. (10) and (15)) which reflect two-center interference phenomenon cancels each other out as a result of the incoherent sum. While the $\boldsymbol{\kappa}$ -dependence originated from MFPAD, $I^{g/u}$, in $\langle t_{\partial \kappa}(E1'; \mathbf{k}, \hat{\epsilon}) \rangle_{\text{IC}}$ disappears, $\langle t_{\partial \kappa}(E1'; \mathbf{k}, \hat{\epsilon}) \rangle_{\text{IC}}$ keeps the $\boldsymbol{\kappa}$ -dependent factor, which is not originated from the two-center interference phenomenon.

We found the following relations between the differences in the MFPAD and photoemission time delay in the two opposite directions $\hat{\mathbf{k}}$ and $-\hat{\mathbf{k}}$:

$$\langle I(E1'; \mathbf{k}, \hat{\epsilon}) \rangle_{\text{IC}} - \langle I(E1'; -\mathbf{k}, \hat{\epsilon}) \rangle_{\text{IC}} = 0 \quad (23)$$

$$\begin{aligned} \langle t(E1'; \mathbf{k}, \hat{\epsilon}, \boldsymbol{\kappa}) \rangle_{\text{IC}} - \langle t(E1'; -\mathbf{k}, \hat{\epsilon}, \boldsymbol{\kappa}) \rangle_{\text{IC}} \\ = 2 \langle t_{\partial \kappa}(E1'; \mathbf{k}, \hat{\epsilon}, \boldsymbol{\kappa}) \rangle_{\text{IC}}. \end{aligned} \quad (24)$$

The proofs of these equations are provided in Appendix A. The relation of Eq. (24) makes it possible to extract the non-dipole effect.

D. Decomposition of the photoemission time delay using Multiple Scattering theory with spherical wave correction

In our previous study on heteronuclear diatomic molecules, the photoemission time delay was decomposed into three contributions, atomic, propagation and scattering terms, by expanding the photoionization amplitude in the scattering order based on Multiple Scattering theory. [47] We follow this method to expand the photoionization amplitude A_i in Eq. (6) with the help of Muffin-tin approximation [47] which uses spherically symmetric potentials.

The exited photoelectron from site i is emitted directly, singly scattered, doubly scattered or multiply scattered, we obtain the following expansion as a result:

$$\begin{aligned} A_i(E1; \mathbf{k}, \hat{\epsilon}) \xrightarrow{\text{Multiple Scattering}} -M_{L_c}^1(E1; k) i \sqrt{\frac{k}{\pi}} T_1(k) \\ \times \{D_i(\mathbf{k}, \hat{\epsilon}) + S_{i \rightarrow j}(\mathbf{k}, \hat{\epsilon}) + H_{i \rightleftharpoons j}(\mathbf{k}, \hat{\epsilon})\} \\ \equiv \bar{A}_i(E1; \mathbf{k}, \hat{\epsilon}), \end{aligned} \quad (25)$$

where $M_{L_c}^1(E1; k)$ is the transition matrix element describing the excitation from the core orbital of atom i within $E1$ transition approximation and T_1 is T -matrix (transition operator) for a partial wave of $l = 1$ with the spherical potential of site i . D_i represents the contribution of photoelectrons directly emitted from site i . $S_{i \rightarrow j}$ is the single scattering contribution for photoelectrons emitted from site i propagating to and being scattered by site j . $H_{i \rightleftharpoons j}$ is the higher order scattering contribution for photoelectrons between site i and j , then emitted from either site i or j . Here, D_i and $S_{i \rightarrow j}$ are:

$$D_i(\mathbf{k}, \hat{\epsilon}) = \cos \theta_{\hat{\epsilon}, \hat{\mathbf{k}}} e^{-i\mathbf{k} \cdot \mathbf{R}_{i0}} \quad (26)$$

and

$$\begin{aligned} S_{i \rightarrow j}(\mathbf{k}, \hat{\epsilon}) = \cos \theta_{\hat{\epsilon}, \hat{\mathbf{R}}_{ji}} \mathcal{G}(k, R_{ji}) f^{(0)}(\mathbf{k}, \mathbf{R}_{ji}) e^{i\mathbf{k} \cdot \mathbf{R}_{i0}} \\ + \sin \theta_{\hat{\epsilon}, \hat{\mathbf{R}}_{ji}} \cos \phi_{\hat{\epsilon}, \hat{\mathbf{R}}_{ji}, \hat{\mathbf{k}}} \mathcal{G}(k, R_{ji}) f^{(1)}(\mathbf{k}, \mathbf{R}_{ji}) e^{i\mathbf{k} \cdot \mathbf{R}_{i0}}, \end{aligned} \quad (27)$$

where $\theta_{\hat{\mathbf{r}}, \hat{\mathbf{r}}'} = \arccos(\hat{\mathbf{r}} \cdot \hat{\mathbf{r}}')$ and $\phi_{\hat{\epsilon}, \hat{\mathbf{R}}_{ji}, \hat{\mathbf{k}}}$ is the dihedral angle between the plane containing $\hat{\epsilon}$ and $\hat{\mathbf{R}}_{ji}$ and the plane containing $\hat{\mathbf{R}}_{ji}$ and $\hat{\mathbf{k}}$. When $\hat{\epsilon}$, $\hat{\mathbf{R}}$ and $\hat{\mathbf{k}}$ are on the same plane, $\phi_{\hat{\epsilon}, \hat{\mathbf{R}}_{ji}, \hat{\mathbf{k}}} = 0$. This condition is employed for numerical calculation in Section III. \mathbf{R}_{ji} is the position vector from the center position of site i to j . $\mathcal{G}(k, R) \equiv e^{ikR}/R$ is free electron green's function. $f^{(0)}$ and $f^{(1)}$ are modified scattering amplitudes, including the spherical wave effects. The details of the derivations are given in Appendix B and Ref. [52].

Let us briefly discuss the contribution of spherical wave components on Eq. (27). The first term in Eq. (27) describes the contribution from the photoelectron exited by the polarization component parallel to the molecular axis and only consist to the plane wave term at the plane wave

limit: The spherical correction factors $c_l(kR)$ defined as Eq. (B6) in Appendix B reaches $c_l(kR) \rightarrow 1$. Contrary to the first term, the second term in Eq. (27) represents the contribution from the photoelectron excited by the polarization component perpendicular to the molecular axis propagating to the next atom. When the polarization vector κ is perpendicular to the molecular axis, the

Using the expansion described in Eqs. (25)-(27), k -partial derivative part of the photoemission time delay, $t_{\partial k}^{g/u}$, in Eq. (16) can be divided into three components,

$$t_{\partial k}^{g/u}(E1'; \mathbf{k}, \hat{\boldsymbol{\epsilon}}, \boldsymbol{\kappa}) \xrightarrow{\text{Multiple Scattering}} t_{\text{abs}}(E1; k) + t_{\text{path}}^{g/u}(E1'; \mathbf{k}, \hat{\boldsymbol{\epsilon}}, \boldsymbol{\kappa}) + t_{\text{sc}}^{g/u}(E1'; \mathbf{k}, \hat{\boldsymbol{\epsilon}}, \boldsymbol{\kappa}), \quad (28)$$

where

$$t_{\text{abs}}(E1; k) \equiv \frac{1}{v_g} \frac{\partial}{\partial k} \arg \{ M_{L_c}^1(E1; k) T_1(k) \}, \quad (29)$$

$$\begin{aligned} t_{\text{path}}^{g/u}(E1'; \mathbf{k}, \hat{\boldsymbol{\epsilon}}, \boldsymbol{\kappa}) &\equiv \left| \bar{A}^{g/u}(E1'; \mathbf{k}, \hat{\boldsymbol{\epsilon}}, \boldsymbol{\kappa}) \right|^{-2} \times \text{Im} \left\{ \bar{A}^{g/u*}(E1'; \mathbf{k}, \hat{\boldsymbol{\epsilon}}, \boldsymbol{\kappa}) \frac{-1}{\sqrt{2}} M_{L_c}^1(E1; k) i \sqrt{\frac{k}{\pi}} T_1(k) \right. \\ &\times \left(\left[e^{-i\boldsymbol{\kappa} \cdot \frac{\mathbf{R}}{2}} \cos \theta_{\hat{\boldsymbol{\epsilon}}, \hat{\mathbf{k}}} \frac{1}{v_g} \frac{\partial}{\partial k} \left(e^{-i\mathbf{k} \cdot \frac{\mathbf{R}}{2}} \right) \pm e^{i\boldsymbol{\kappa} \cdot \frac{\mathbf{R}}{2}} \cos \theta_{\hat{\boldsymbol{\epsilon}}, \hat{\mathbf{k}}} \frac{1}{v_g} \frac{\partial}{\partial k} \left(e^{i\mathbf{k} \cdot \frac{\mathbf{R}}{2}} \right) \right] \right. \\ &+ \left[e^{-i\boldsymbol{\kappa} \cdot \frac{\mathbf{R}}{2}} \left\{ \cos \theta_{\hat{\boldsymbol{\epsilon}}, \hat{\mathbf{R}}} \frac{1}{v_g} \frac{\partial}{\partial k} \left(\mathcal{G}(k, R) e^{-i\mathbf{k} \cdot \frac{\mathbf{R}}{2}} \right) f^{(0)}(\mathbf{k}, -\mathbf{R}) + \sin \theta_{\hat{\boldsymbol{\epsilon}}, \hat{\mathbf{R}}} \cos \phi_{\hat{\boldsymbol{\epsilon}}, \hat{\mathbf{R}}, \hat{\mathbf{k}}} \frac{1}{v_g} \frac{\partial}{\partial k} \left(\mathcal{G}(k, R) e^{-i\mathbf{k} \cdot \frac{\mathbf{R}}{2}} \right) f^{(1)}(\mathbf{k}, -\mathbf{R}) \right\} \right. \\ &\quad \left. \pm e^{i\boldsymbol{\kappa} \cdot \frac{\mathbf{R}}{2}} \left\{ \cos \theta_{\hat{\boldsymbol{\epsilon}}, -\hat{\mathbf{R}}} \frac{1}{v_g} \frac{\partial}{\partial k} \left(\mathcal{G}(k, R) e^{i\mathbf{k} \cdot \frac{\mathbf{R}}{2}} \right) f^{(0)}(\mathbf{k}, \mathbf{R}) + \sin \theta_{\hat{\boldsymbol{\epsilon}}, -\hat{\mathbf{R}}} \cos \phi_{\hat{\boldsymbol{\epsilon}}, -\hat{\mathbf{R}}, \hat{\mathbf{k}}} \frac{1}{v_g} \frac{\partial}{\partial k} \left(\mathcal{G}(k, R) e^{i\mathbf{k} \cdot \frac{\mathbf{R}}{2}} \right) f^{(1)}(\mathbf{k}, \mathbf{R}) \right\} \right] \\ &+ \dots \left. \right) \left. \right\}, \quad (30) \end{aligned}$$

$$\begin{aligned} t_{\text{sc}}^{g/u}(E1'; \mathbf{k}, \hat{\boldsymbol{\epsilon}}, \boldsymbol{\kappa}) &\equiv \left| \bar{A}^{g/u}(E1'; \mathbf{k}, \hat{\boldsymbol{\epsilon}}, \boldsymbol{\kappa}) \right|^{-2} \times \text{Im} \left\{ \bar{A}^{g/u*}(E1'; \mathbf{k}, \hat{\boldsymbol{\epsilon}}, \boldsymbol{\kappa}) \frac{-1}{\sqrt{2}} M_{L_c}^1(E1; k) i \sqrt{\frac{k}{\pi}} T_1(k) \right. \\ &\times \left(\left[e^{-i\boldsymbol{\kappa} \cdot \frac{\mathbf{R}}{2}} \left\{ \cos \theta_{\hat{\boldsymbol{\epsilon}}, \hat{\mathbf{R}}} \mathcal{G}(k, R) e^{-i\mathbf{k} \cdot \frac{\mathbf{R}}{2}} \frac{1}{v_g} \frac{\partial}{\partial k} \left(f^{(0)}(\mathbf{k}, -\mathbf{R}) \right) + \sin \theta_{\hat{\boldsymbol{\epsilon}}, \hat{\mathbf{R}}} \cos \phi_{\hat{\boldsymbol{\epsilon}}, \hat{\mathbf{R}}, \hat{\mathbf{k}}} \mathcal{G}(k, R) e^{-i\mathbf{k} \cdot \frac{\mathbf{R}}{2}} \frac{1}{v_g} \frac{\partial}{\partial k} \left(f^{(1)}(\mathbf{k}, -\mathbf{R}) \right) \right\} \right. \\ &\quad \left. \pm e^{i\boldsymbol{\kappa} \cdot \frac{\mathbf{R}}{2}} \left\{ \cos \theta_{\hat{\boldsymbol{\epsilon}}, -\hat{\mathbf{R}}} \mathcal{G}(k, R) e^{i\mathbf{k} \cdot \frac{\mathbf{R}}{2}} \frac{1}{v_g} \frac{\partial}{\partial k} \left(f^{(0)}(\mathbf{k}, \mathbf{R}) \right) + \sin \theta_{\hat{\boldsymbol{\epsilon}}, -\hat{\mathbf{R}}} \cos \phi_{\hat{\boldsymbol{\epsilon}}, -\hat{\mathbf{R}}, \hat{\mathbf{k}}} \mathcal{G}(k, R) e^{i\mathbf{k} \cdot \frac{\mathbf{R}}{2}} \frac{1}{v_g} \frac{\partial}{\partial k} \left(f^{(1)}(\mathbf{k}, \mathbf{R}) \right) \right\} \right] \\ &+ \dots \left. \right) \left. \right\} \quad (31) \end{aligned}$$

and

$$\bar{A}^{g/u}(E1'; \mathbf{k}, \hat{\boldsymbol{\epsilon}}, \boldsymbol{\kappa}) \equiv \frac{1}{\sqrt{2}} \left(e^{-i\boldsymbol{\kappa} \cdot \frac{\mathbf{R}}{2}} \bar{A}_1(E1; \mathbf{k}, \hat{\boldsymbol{\epsilon}}) \pm e^{i\boldsymbol{\kappa} \cdot \frac{\mathbf{R}}{2}} \bar{A}_2(E1; \mathbf{k}, \hat{\boldsymbol{\epsilon}}) \right). \quad (32)$$

Here, t_{abs} corresponds to the atomic time delay for absorbing atoms within $E1$ transition approximation. It is independent of the photoemission and light angles. $t_{\text{path}}^{g/u}$ and $t_{\text{sc}}^{g/u}$ are time delays due to the propagation of photoelectrons between atoms and scattering of photoelectrons by atoms, respectively.

E. Direct Wave contribution D_i for MFPAD and photoemission time delay

We consider the simplest Direct Wave approximation, which neglects scatterings of photoelectrons and describes the photoelectron wave function as the superposition of direct waves from atoms. In this approximation, we only

propagation time of the light between atoms becomes maximum; however, this term vanishes in Plane Wave approximation because only the spherical contribution describes the propagation of the wave along the molecular axis. To consider this contribution, spherical wave formalism is employed.

consider the lowest term D_i in Eq. (25). As a result, we obtain the following analytical expression for MFPAD:

$$I^{g/u}(E1'; \mathbf{k}, \hat{\mathbf{e}}, \boldsymbol{\kappa}) \xrightarrow{\text{Direct Wave approximation}} 16\pi c\kappa k |M_{L_c}^1(k) T_1(k)|^2 (\hat{\mathbf{e}} \cdot \hat{\mathbf{k}})^2 [1 \pm \cos\{(\mathbf{k} - \boldsymbol{\kappa}) \cdot \mathbf{R}\}]. \quad (33)$$

This is an expression for two-center interference phenomenon shifted by $\boldsymbol{\kappa} \cdot \mathbf{R}$ due to non-dipole effects and is a corresponding result reported by Ivanov *et al.* [44].

Conversely, the photoemission time delay within Direct Wave approximation is equal to that of the single absorbing atom and does not exhibit the properties of molecular structure such as angular dependence and the non-dipole effect:

$$t^{g/u}(E1'; \mathbf{k}, \hat{\mathbf{e}}, \boldsymbol{\kappa}) \xrightarrow{\text{Direct Wave approximation}} t_{\text{abs}}(E1; k). \quad (34)$$

It is therefore necessary to describe the photoemission time delay in a model that considers the effects of scattering with the surrounding atoms unlike MFPADs.

III. RESULTS AND DISCUSSION

A. Analytical expression in high energy region

From our previous study of the photoemission time delay of heteronuclear diatomic molecules [47], we expect that $t_{\text{path}}^{g/u(1)}$ and $\langle t_{\text{path}}^{(1)} \rangle_{\text{IC}}$ (the superscript (1) denotes Single Scattering approximation) are dominant in the photoemission time delays $t^{g/u}$ and $\langle t \rangle_{\text{IC}}$ in the high energy region. Finally, we reached the following analytical expressions:

$$t_{\text{path}}^{g/u(1)}(E1'; \mathbf{k}, \hat{\mathbf{e}}, \boldsymbol{\kappa}) = \frac{2 \langle I^{(1)}(E1; \mathbf{k}, \hat{\mathbf{e}}) \rangle_{\text{IC}} \langle t_{\text{path}}^{(1)}(E1; \mathbf{k}, \hat{\mathbf{e}}) \rangle_{\text{IC}}}{I^{g/u(1)}(E1'; \mathbf{k}, \hat{\mathbf{e}}, \boldsymbol{\kappa})} \pm \frac{\alpha(k)}{I^{g/u(1)}(E1'; \mathbf{k}, \hat{\mathbf{e}}, \boldsymbol{\kappa})} \\ \times \frac{R}{v_g} \left[(1 + \hat{\mathbf{k}} \cdot \hat{\mathbf{R}}) \text{Re} \{ D_1^*(\mathbf{k}, \hat{\mathbf{e}}) S_{2 \rightarrow 1}(\mathbf{k}, \hat{\mathbf{e}}) \} + (1 - \hat{\mathbf{k}} \cdot \hat{\mathbf{R}}) \text{Re} \{ D_2^*(\mathbf{k}, \hat{\mathbf{e}}) S_{1 \rightarrow 2}(\mathbf{k}, \hat{\mathbf{e}}) \} \right. \\ \left. + 2 \text{Re} \{ S_{1 \rightarrow 2}^*(\mathbf{k}, \hat{\mathbf{e}}) S_{2 \rightarrow 1}(\mathbf{k}, \hat{\mathbf{e}}) \} \right], \quad (35)$$

and

$$\langle t_{\text{path}}^{(1)}(E1; \mathbf{k}, \hat{\mathbf{e}}) \rangle_{\text{IC}} = \frac{I_1^{(1)}(E1; \mathbf{k}, \hat{\mathbf{e}}) t_{\text{path},1}^{(1)}(E1; \mathbf{k}, \hat{\mathbf{e}}) + I_2^{(1)}(E1; \mathbf{k}, \hat{\mathbf{e}}) t_{\text{path},2}^{(1)}(E1; \mathbf{k}, \hat{\mathbf{e}})}{2 \langle I^{(1)}(E1; \mathbf{k}, \hat{\mathbf{e}}) \rangle_{\text{IC}}}, \quad (36)$$

where

$$t_{\text{path},i}^{(1)}(E1; \mathbf{k}, \hat{\mathbf{e}}) \equiv \frac{R}{v_g} \left(1 - \hat{\mathbf{k}} \cdot \hat{\mathbf{R}}_{ji} \right) \frac{1}{2} \left(1 - \frac{|D_i(\mathbf{k}, \hat{\mathbf{e}})|^2 - |S_{i \rightarrow j}(\mathbf{k}, \hat{\mathbf{e}})|^2}{(\alpha(k))^{-1} I_i^{(1)}(E1; \mathbf{k}, \hat{\mathbf{e}})} \right), \quad (37)$$

$$I^{g/u(1)}(E1'; \mathbf{k}, \hat{\mathbf{e}}, \boldsymbol{\kappa}) = \langle I^{(1)}(E1; \mathbf{k}, \hat{\mathbf{e}}) \rangle_{\text{IC}} \\ \pm \alpha(k) \left[\text{Re} \left\{ e^{i\boldsymbol{\kappa} \cdot \mathbf{R}} D_1^*(\mathbf{k}, \hat{\mathbf{e}}) D_2(\mathbf{k}, \hat{\mathbf{e}}) \right\} + \text{Re} \left\{ e^{i\boldsymbol{\kappa} \cdot \mathbf{R}} D_1^*(\mathbf{k}, \hat{\mathbf{e}}) S_{2 \rightarrow 1}(\mathbf{k}, \hat{\mathbf{e}}) \right\} \right. \\ \left. + \text{Re} \left\{ e^{i\boldsymbol{\kappa} \cdot \mathbf{R}} S_{1 \rightarrow 2}^*(\mathbf{k}, \hat{\mathbf{e}}) D_2(\mathbf{k}, \hat{\mathbf{e}}) \right\} + \text{Re} \left\{ e^{i\boldsymbol{\kappa} \cdot \mathbf{R}} S_{1 \rightarrow 2}^*(\mathbf{k}, \hat{\mathbf{e}}) S_{2 \rightarrow 1}(\mathbf{k}, \hat{\mathbf{e}}) \right\} \right], \quad (38)$$

$$\langle I^{(1)}(E1; \mathbf{k}, \hat{\mathbf{e}}) \rangle_{\text{IC}} = \frac{1}{2} \left(I_1^{(1)}(E1; \mathbf{k}, \hat{\mathbf{e}}) + I_2^{(1)}(E1; \mathbf{k}, \hat{\mathbf{e}}) \right), \quad (39)$$

$$I_i^{(1)}(E1; \mathbf{k}, \hat{\mathbf{e}}) = \alpha(k) \left[|D_i(\mathbf{k}, \hat{\mathbf{e}})|^2 + |S_{i \rightarrow j}(\mathbf{k}, \hat{\mathbf{e}})|^2 + 2 \text{Re} \{ D_i^*(\mathbf{k}, \hat{\mathbf{e}}) S_{i \rightarrow j}(\mathbf{k}, \hat{\mathbf{e}}) \} \right], \quad (40)$$

$$\alpha(k) \equiv 8\pi c\kappa k |M_{L_c}^1(E1; k) T_1(k)|^2. \quad (41)$$

Here, $t_{\text{path},i}^{(1)}$ is the same as that obtained for the excitation from localized core orbital in atomic site i of the

heteronuclear diatomic molecules (Eq. (20) in Ref. [47]) except spherical wave correction.

Next, we show numerically calculated results of the MFPAD and photoemission time delay of nitrogen molecules for two cases: (I) light incident direction $\hat{\kappa}$ parallel to the molecular axis $\hat{\mathbf{R}}$ and (II) perpendicular to the molecular axis $\hat{\mathbf{R}}$ in $\hat{\mathbf{e}}-\hat{\kappa}$ plane (see Fig. 2). The numerical results in the both cases are compared with the above analytical expressions to verify their validity (Figs. 3 and 5). The numerical results were obtained as

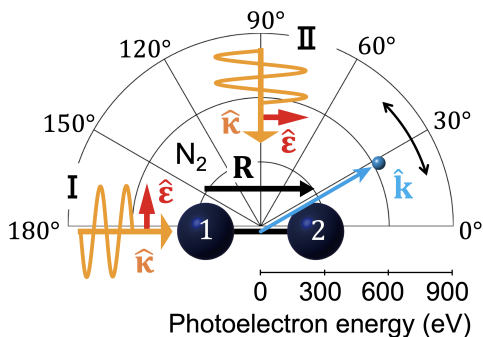


FIG. 2. Definition of the molecular frame for nitrogen molecule with two different directions of incident light $\hat{\kappa}$, which are (I) parallel and (II) perpendicular to the molecular axis $\hat{\mathbf{R}}$. The photoemission direction $\hat{\mathbf{k}}$ and molecular axis $\hat{\mathbf{R}}$ are in $\hat{\mathbf{e}}-\hat{\kappa}$ plane, where $\hat{\mathbf{e}}$ is the polarization vector of incident light. The radius of the semicircle gives the photoelectron energy $E_{\mathbf{k}}$. The polar angles give the photoemission direction $\hat{\mathbf{k}}$ relative to the molecular axis $\hat{\mathbf{R}}$. We use such polar plots in Figs. 3-5.

follows:

- (i) Perform multiple scattering calculations for A_i defined in Eq. (7) by MsSpec code [53] within Muffin-tin approximation.
- (ii) Calculate photoionization amplitude $A^{g/u}$ based on Eq. (6).
- (iii) Calculate the MFPAD and photoemission time delay in terms of Eqs. (9) and (12), respectively.
- (iv) Take their incoherent sums as the definitions in Eqs. (18) and (19), respectively.
- (v) Subtract t_{abs} from each photoemission time delay.

The quantities obtained from step (v) correspond to the difference in the photoemission time delay between the nitrogen molecule and the nitrogen atom, namely $t^{g/u} - t_{\text{abs}}$ and $\langle t \rangle_{\text{IC}} - t_{\text{abs}}$, which are measurable values in the experiment [40]. Our numerical and analytical results exclude the effect of the Coulomb tail because the molecular potential is approximated by two touching atomic spheres and the null potential rest of the space in Muffin-tin approximation as in our previous study [47]. However, we expect that it can be negligible because the

Coulomb tail effects of the molecule and atom are almost well canceled out in step (v). we used the ground state potential numerically constructed by superposition of atomic potentials which is self-consistently calculated with neglecting the core-holes. This does not make any substantial changes on our discussions in the high energy region.

B. Light incident parallel to the molecular axis ($\hat{\kappa} \parallel \hat{\mathbf{R}}$)

The contribution of this non-dipole effect is most enhanced when the direction of light $\hat{\kappa}$ is parallel to the molecular axis $\hat{\mathbf{R}}$ because propagation time of light between atoms is maximum. This is a case where the analytical expression cannot be managed by Plane Wave approximation: In Eq. (27), a first term (mostly contribution from plane waves) vanishes but a second term (mostly contribution from spherical waves) is maximized in the single scattering wave described.

The analytical expressions for the MFPAD (Eqs. (38) and (39) and photoemission time delay (Eqs. (35) and (36)) reproduce the numerical results in the high energy region well. by comparing the numerical and analytical results (upper and lower semicircle of polar plots in Fig. 3, respectively). The MFPAD peaks exhibit tilts due to the non-dipole effect when the photoelectrons from *gerade* and *ungerade* states are distinguished, as shown in Fig. 3(a) and (b). These tilt angles can be estimated using Eq. (33) based on Direct Wave approximation. Fig. 3(c) shows that the incoherent sum of the MFPAD which is independent from κ as in Eq. (20) does not show such tilting. The photoemission time delays for the *gerade* and *ungerade* states have large peaks at energies and angles where the MFPADs are minimal (See Fig. 3(d) and (e)) because the analytical expression for the t_{path} for these states (Eqs. (35)) and that of the corresponding incoherent sum (Eq. (36)) are proportional to the inverse of the MFPAD. In Fig. 3(f), we see that the prominent peaks disappear after taking the incoherent sum of the photoemission time delays.

Figure 3(f) looks symmetric with respect to the plane perpendicular to the direction of the incident light $\hat{\kappa}$. Actually, the lower semicircle of the analytical result ($\langle t_{\text{path}}^{(1)}(E1; \mathbf{k}, \hat{\mathbf{e}}) \rangle_{\text{IC}}$) is symmetric because $\hat{\kappa}$ -dependence is canceled out by taking an incoherent sum. However, the upper semicircle of the incoherent sum of the total photoemission time delays ($\langle t(E1'; \mathbf{k}, \hat{\mathbf{e}}, \kappa) \rangle_{\text{IC}}$) is asymmetric. We adopt the difference of the upper semicircle in Fig. 3(f) between in any emission direction, $\hat{\mathbf{k}}$, and in the opposite direction, $-\hat{\mathbf{k}}$, then we see the results in Fig. 4 that there remain zeptosecond differences. This zeptosecond asymmetry is estimated to be twice the κ -partial derivative part of the photoemission time delay, $2 \langle t_{\partial\kappa}(E1'; \mathbf{k}, \hat{\mathbf{e}}, \kappa) \rangle_{\text{IC}}$, in our theoretical framework as in Eq. (24).

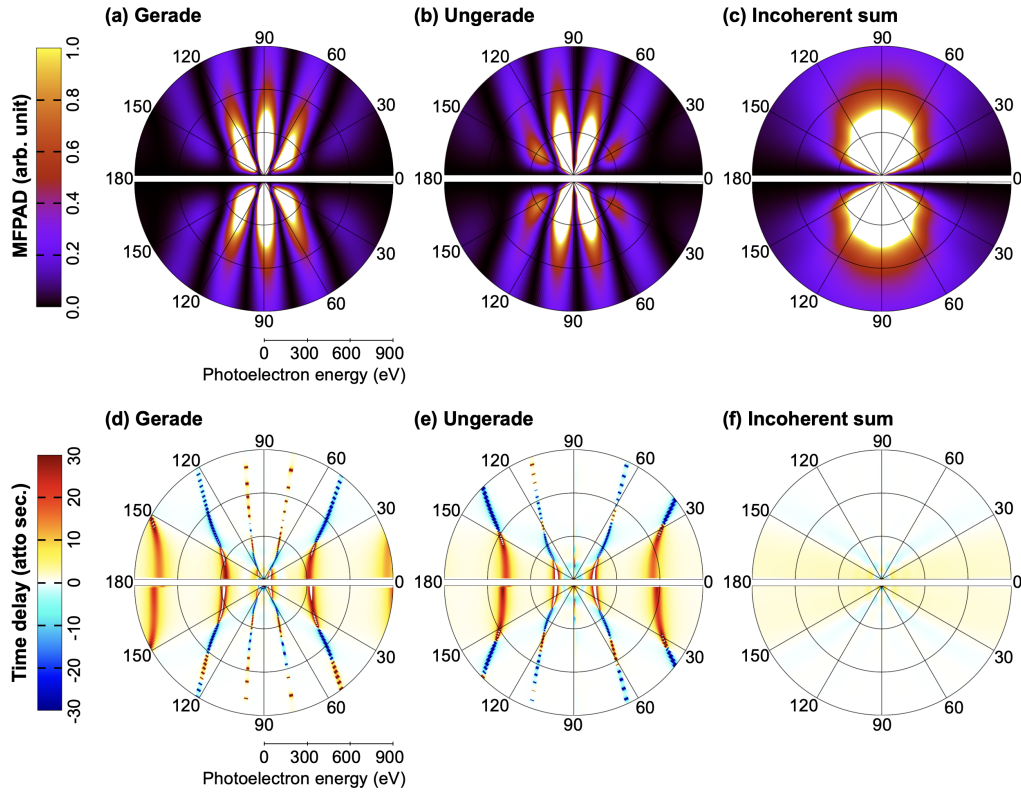


FIG. 3. Comparison of numerical and analytical results for MFPAD and photoemission time delay from *gerade* and *ungerade* state of $1s$ core orbitals in nitrogen molecules in the coordinate system (I) in Fig. 2 ($\hat{\kappa} \parallel \hat{\mathbf{R}}$) in terms of energy and angle dependence of the photoelectrons. The upper semicircles in the polar plots are full multiple scattering numerical calculation results of MFPAD for (a) *gerade* and (b) *ungerade* states, $I^{g/u}(E1'; \mathbf{k}, \hat{\mathbf{e}}, \boldsymbol{\kappa})$, and (c) their incoherent sum $\langle I(E1'; \mathbf{k}, \hat{\mathbf{e}}) \rangle_{\text{IC}}$. Difference in the photoemission time delay between nitrogen molecule and nitrogen atom for (d) *gerade* and (e) *ungerade* states, $t^{g/u}(E1'; \mathbf{k}, \hat{\mathbf{e}}, \boldsymbol{\kappa}) - t_{\text{abs}}(E1; k)$, and (f) their incoherent sum, $\langle t(E1'; \mathbf{k}, \hat{\mathbf{e}}) \rangle_{\text{IC}} - t_{\text{abs}}(E1; k)$. The lower semicircles in the polar plots are the analytical results of MFPAD for (a) *gerade* and (b) *ungerade* states, $I^{g/u(1)}(E1'; \mathbf{k}, \hat{\mathbf{e}}, \boldsymbol{\kappa})$, in Eq. (38), and (c) their incoherent sum, $\langle I^{(1)}(E1'; \mathbf{k}, \hat{\mathbf{e}}) \rangle_{\text{IC}}$, in Eq. (39). Difference in the photoemission time delay between nitrogen molecule and nitrogen atom for (d) *gerade* and (e) *ungerade* states, $t_{\text{path}}^{g/u(1)}(E1'; \mathbf{k}, \hat{\mathbf{e}}, \boldsymbol{\kappa})$, in Eq. (35), and (f) their incoherent sum, $\langle t_{\text{path}}^{(1)}(E1'; \mathbf{k}, \hat{\mathbf{e}}) \rangle_{\text{IC}}$, in Eq. (36).

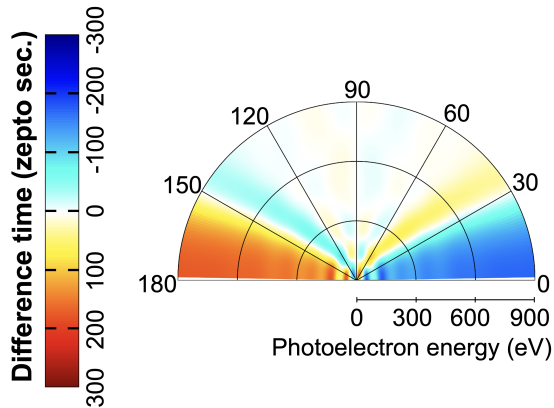


FIG. 4. The difference between the full multiple scattering numerical calculation results of the incoherent sum of photoemission time delays (upper semicircle in Fig. 3(f)) in any emission direction and the opposite direction, $\langle t(E1'; \mathbf{k}, \hat{\mathbf{e}}, \boldsymbol{\kappa}) \rangle_{\text{IC}} - \langle t(E1'; -\mathbf{k}, \hat{\mathbf{e}}, \boldsymbol{\kappa}) \rangle_{\text{IC}}$.

C. Light incident perpendicular to the molecular axis ($\hat{\kappa} \perp \hat{\mathbf{R}}$)

When the direction of light $\boldsymbol{\kappa}$ is perpendicular to the molecular axis $\hat{\mathbf{R}}$, the non-dipole effect disappears. This can be observed from Eq. (6): the non-dipole factor $\exp\{\pm i\boldsymbol{\kappa} \cdot \mathbf{R}/2\}$ becomes 1. Consequently, forward and backward asymmetries in the MFPAD and photoemission time delay along the direction of the incident light vanish. In this case, the second term in Eq. (27) (mostly spherical wave component) also vanishes.

In the high energy region, the analytical expressions within Plane Wave approximation (lower semicircle in Fig. 5) can explain the behavior of the numerical results of the MFPAD and the photoemission time delay (upper semicircle in Fig. 5).

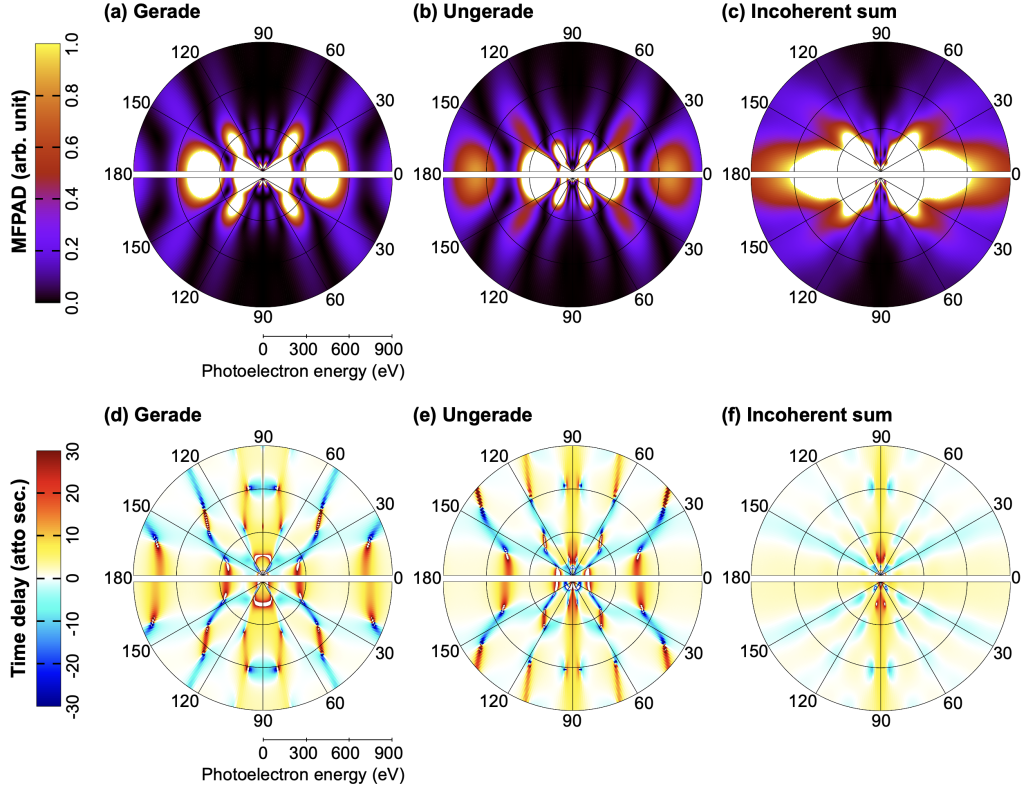


FIG. 5. Comparison of numerical and analytical results for MFPAD and photoemission time delay from *gerade* and *ungerade* state of $1s$ core orbitals in nitrogen molecules in the coordinate system (II) in Fig. 2 ($\hat{\kappa} \perp \hat{\mathbf{R}}$) in terms of energy and angle dependence of the photoelectrons. The upper semicircles in the polar plots are full multiple scattering numerical calculation results of MFPAD for (a) *gerade* and (b) *ungerade* states, $I^{g/u}(E1'; \mathbf{k}, \hat{\mathbf{e}}, \boldsymbol{\kappa})$, and (c) their incoherent sum, $\langle I(E1; \mathbf{k}, \hat{\mathbf{e}}) \rangle_{\text{IC}}$. Difference in the photoemission time delay between nitrogen molecule and nitrogen atom for (d) *gerade* and (e) *ungerade* states, $t^{g/u}(E1'; \mathbf{k}, \hat{\mathbf{e}}, \boldsymbol{\kappa}) - t_{\text{abs}}(E1; k)$, and (f) their incoherent sum, $\langle t(E1; \mathbf{k}, \hat{\mathbf{e}}) \rangle_{\text{IC}} - t_{\text{abs}}(E1; k)$. The lower semicircles in the polar plots are the analytical results within Plane Wave approximation, Eq. (B14), of MFPAD for (a) *gerade* and (b) *ungerade* states, $I^{g/u(1)}(E1'; \mathbf{k}, \hat{\mathbf{e}}, \boldsymbol{\kappa})$, in Eq. (38), and (c) their incoherent sum, $\langle I^{(1)}(E1; \mathbf{k}, \hat{\mathbf{e}}) \rangle_{\text{IC}}$, in Eq. (39). Difference in the photoemission time delay between nitrogen molecule and nitrogen atom for (d) *gerade* and (e) *ungerade* states, $t_{\text{path}}^{g/u(1)}(E1'; \mathbf{k}, \hat{\mathbf{e}}, \boldsymbol{\kappa})$, in Eq. (35), and (f) their incoherent sum, $\langle t_{\text{path}}^{(1)}(E1; \mathbf{k}, \hat{\mathbf{e}}) \rangle_{\text{IC}}$, in Eq. (36).

IV. CONCLUSION

In this paper, we investigated the non-dipole effect in core-level photoemission of homonuclear diatomic molecules by introducing a theoretical model beyond Electric Dipole approximation. We first described the core-level MFPAD and photoemission time delay using the LCAO method. We then introduced $E1'$ approximation to investigate the non-dipole effect in the MFPAD and the photoemission time delay. These approximations allowed us to divide a term $t_{\partial k}^{g/u}$, which is proportional to the attosecond-order interatomic propagation time of photoelectrons R/v_g , and a term $t_{\partial \kappa}^{g/u}$, which is proportional to the zeptosecond-order interatomic propagation time of light R/c . This $t_{\partial \kappa}^{g/u}$ has zeptosecond temporal information specific to the photoemission time delay, which the MFPAD does not have. Furthermore, we analytically derived the fundamental relations for $\langle I \rangle_{\text{IC}}$ in Eq. (23) and $\langle t \rangle_{\text{IC}}$ in Eq. (24).

Next, $t_{\partial k}^{g/u}$ was divided into an atomic time delay of a single absorbing atom t_{abs} and molecule-specific delays due to photoelectron propagation, $t_{\text{path}}^{g/u}$, and scattering, $t_{\text{sc}}^{g/u}$ by describing the photoelectron scattering state in the framework of Multiple Scattering theory. We found that the molecule-specific delays $t_{\text{path}}^{g/u}$ and $t_{\text{sc}}^{g/u}$, and $t_{\partial \kappa}^{g/u}$ disappear in high energy region where the single scattering approximation is valid. We also derived analytical expressions (Eqs. (35-41)) for the photoemission time delay in the high energy region by considering up to the single scattering. The validity of these analytical expressions was confirmed by comparison with the full multiple scattering numerical results for nitrogen molecule.

The photoemission time delay includes real-time information on the zeptosecond-scale dynamics of the interaction of light with molecules. In addition, the photoemission time delay has information of the molecular potential because the scattering contribution plays an important role. Our theoretical results indicate the possibil-

ity of accessing information beyond MFPAD from measurement of the photoemission time delay with future improvements in ultrashort light sources and detection technology. This study will also be a basis of theoretical studies of photoionization phenomena in extended nano systems with many identical atoms such as large polyatomic molecules and condensed matters (liquids and solids) to examine their photoemission time delays and non-dipole effects.

ACKNOWLEDGMENTS

We would like to thank Mr. S. Sakamoto for fruitful discussion. We would like to thank Prof. Y. Hikosaka for careful reading. This work was supported by JST, the establishment of university fellowships toward the creation of science and technology innovation, Grant Number JPMJFS2115. K. Y. is grateful for the financial support from JSPS KAKENHI Grant Number 19H05628. This work was supported by JST, CREST Grant Number JPMJCR1861, Japan.

Appendix A: Proof of the relationships between two opposite directions of photoelectrons for the incoherent sums of the MFPAD and photoemission time delay

We have the following basic relationships:

$$I_1(E1; \mathbf{k}, \hat{\boldsymbol{\epsilon}}) = I_2(E1; -\mathbf{k}, \hat{\boldsymbol{\epsilon}}), \quad (\text{A1})$$

$$t_1(E1; \mathbf{k}, \hat{\boldsymbol{\epsilon}}) = t_2(E1; -\mathbf{k}, \hat{\boldsymbol{\epsilon}}). \quad (\text{A2})$$

These equations can be confirmed from a geometrical point of view: Using symmetry of MFPAD, $I_1(E1; \mathbf{k}, \hat{\boldsymbol{\epsilon}})$ and $t_1(E1; \mathbf{k}, \hat{\boldsymbol{\epsilon}})$ (Fig. (6) (a)) rotated 180 degrees in the $\hat{\boldsymbol{\epsilon}}\text{-}\hat{\mathbf{k}}$ plane and operated as a mirror reflection with respect to the $\hat{\boldsymbol{\epsilon}}\text{-}\hat{\mathbf{k}}$ plane coincide with $I_2(E1; -\mathbf{k}, \hat{\boldsymbol{\epsilon}})$ and $t_2(E1; -\mathbf{k}, \hat{\boldsymbol{\epsilon}})$ (Fig. (6) (b)), respectively. Eqs. (23) and (24) are proven by Eq. (21) with Eqs. (A1) and (A2).

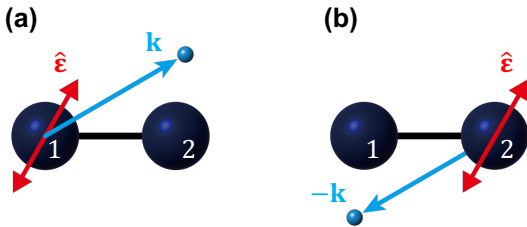


FIG. 6. Photoelectron (a) from site 1 to the direction $\hat{\mathbf{k}}$ and (b) from site 2 to the direction $-\hat{\mathbf{k}}$ excited by linearly polarized light with the polarization vector $\hat{\boldsymbol{\epsilon}}$ for homonuclear diatomic molecules.

Appendix B: Spherical wave correction formalism of Multiple Scattering theory

We here summarize the ingredients to derive Eq. (25) with a help of spherical wave correction formalism in Refs. [52, 54]. The matrix representation of the free electron Green's function is expanded by the method of J. J. Rehr and R. C. Albers [54] as follows:

$$G_{LL'}^{ij} \equiv -4\pi ik \sum_{L''} i^{l+l''-l'} C(L''L'L) h_{l''}(kR_{ij}) \mathcal{Y}_{L''}(\hat{\mathbf{R}}_{ij}) \quad (\text{B1})$$

$$\begin{aligned} &= \sum_{\mu} \sum_{\nu=0}^{|\mu|} \Theta(l-|\mu|) i^l R_{m\mu}^l(\Omega_{\hat{\mathbf{R}}_{ij}}^{-1}) \tilde{\gamma}_{|\mu|\nu}^l(kR_{ij}) \\ &\times \mathcal{G}_{ij}(k) \gamma_{|\mu|\nu}^{l'}(kR_{ij}) R_{\mu m'}^{l'}(\Omega_{\hat{\mathbf{R}}_{ij}}) i^{-l'} \Theta(l'-|\mu|), \end{aligned} \quad (\text{B2})$$

where

$$\tilde{\gamma}_{\mu\nu}^l(kR) = \frac{2l'+1}{N_{l\mu}} \frac{d^{(\nu)}C_l(z)}{dz^{(\nu)}} \frac{z^\nu}{\nu!}, \quad (\text{B3})$$

$$\gamma_{\mu\nu}^{l'}(kR) = -N_{l'\mu} (-1)^\mu \frac{d^{(\mu+\nu)}C_{l'}(z)}{dz^{(\mu+\nu)}} \frac{z^{\mu+\nu}}{(\mu+\nu)!}, \quad (\text{B4})$$

$$N_{l\mu} \equiv (-1)^\mu \sqrt{\frac{2l+1}{4\pi}} \sqrt{\frac{(l-\mu)!}{(l+\mu)!}}, \quad (\text{B5})$$

$$c_l(kR) \equiv \sum_{n=0}^l \frac{i^n}{n!} \frac{(l+n)!}{(2kR)^n (l-n)!}. \quad (\text{B6})$$

$\mathcal{Y}_L(\hat{\mathbf{r}})$ is real spherical harmonics for the angular momentum quantum number $L = (l, m)$, where l is the angular azimuthal quantum number, m is the magnetic quantum number, and $C(L''L'L)$ is Gaunt integral for real spherical harmonics. h_l is Hankel function of the first kind. $R_{m\mu}^l$ is rotation matrix element and $\Omega_{\hat{\mathbf{r}}}$ means rotation that takes the vector $\hat{\mathbf{r}}$ along the z -axis, $\Omega_{\hat{\mathbf{r}}}^{-1}$ is reverse rotation of it. $\mu \geq 0$, $z = 1/(ikR)$ and $C_l(z) = c_l(kR)$. $c_l(kR)$ is the factor of spherical Hankel function: $h_l^+(kR) = i^{-l} \exp(ikR)/(kR) c_l(kR)$.

In the framework of Multiple Scattering theory within Muffin-tin approximation [47], the core-level photoion-

ization amplitude in Eq. (7) can be expanded as follows:

$$\begin{aligned}
A_i(E1; \mathbf{k}, \hat{\mathbf{e}}) &\xrightarrow{\substack{\text{Muffin-tin,} \\ \text{Series Expansion}}} \\
&\sqrt{\frac{k}{\pi}} \frac{4\pi}{3} \sqrt{\frac{1}{4\pi}} M_1^{L_c}(E1; k) \\
&\times \left\{ \sum_n \mathcal{Y}_{1n}(\hat{\mathbf{e}}) T_1^i(k) i^1 \mathcal{Y}_{1n}(-\hat{\mathbf{k}}) e^{-i\mathbf{k}\cdot\mathbf{R}_{iO}} \right. \\
&+ \sum_{j(\neq i)} \sum_{L_1} \sum_n \mathcal{Y}_{1n}(\hat{\mathbf{e}}) T_1^i(k) \\
&\quad \times G_{1nL_1}^{ij} T_{L_1}^j(k) i^{l_1} \mathcal{Y}_{L_1}(-\hat{\mathbf{k}}) e^{-i\mathbf{k}\cdot\mathbf{R}_{jO}} \\
&+ \sum_{k(\neq i)} \sum_{j(\neq k)} \sum_{L_1L_2} \sum_n \mathcal{Y}_{1n}(\hat{\mathbf{e}}) T_1^i(k) \\
&\quad \times G_{1nL_1}^{ik} T_{L_1}^k(k) \\
&\quad \left. \times G_{L_1L_2}^{kj} T_{L_2}^j(k) i^{l_2} \mathcal{Y}_{L_2}(-\hat{\mathbf{k}}) e^{-i\mathbf{k}\cdot\mathbf{R}_{jO}} + \dots \right\}, \quad (\text{B7})
\end{aligned}$$

where

$$M_{L_c}^l(E1; k) \equiv \int_{V_i} dr_i R_l^{i*}(k, r_i) r_i^3 R_{L_c}^l(r_i) \quad (\text{B8})$$

is the transition matrix and T_l^i is the T -matrix element on site i with l . The major contributions from direct and single scattering waves in Eq. (B7) are derived as follows:

$$D_i(\mathbf{k}, \hat{\mathbf{e}}) = \cos \theta_{\hat{\mathbf{e}}, \hat{\mathbf{k}}} e^{-i\mathbf{k}\cdot\mathbf{R}_{iO}} \quad (\text{B9})$$

and

$$\begin{aligned}
S_{i \rightarrow j}(\mathbf{k}, \hat{\mathbf{e}}) &= \cos \theta_{\hat{\mathbf{e}}, \hat{\mathbf{R}}_{ji}} \mathcal{G}(k, R_{ji}) f^{(0)}(\mathbf{k}, \mathbf{R}_{ji}) e^{i\mathbf{k}\cdot\mathbf{R}_{iO}} \\
&+ \sin \theta_{\hat{\mathbf{e}}, \hat{\mathbf{R}}_{ji}} \cos \phi_{\hat{\mathbf{e}}, \hat{\mathbf{R}}_{ji}, \hat{\mathbf{k}}} \mathcal{G}(k, R_{ji}) f^{(1)}(\mathbf{k}, \mathbf{R}_{ji}) e^{i\mathbf{k}\cdot\mathbf{R}_{iO}}, \quad (\text{B10})
\end{aligned}$$

where

$$\begin{aligned}
\cos \phi_{\hat{\mathbf{e}}, \hat{\mathbf{R}}_{ji}, \hat{\mathbf{k}}} &= \frac{\cos \theta_{\hat{\mathbf{e}}, \hat{\mathbf{k}}} - \cos \theta_{\hat{\mathbf{e}}, \hat{\mathbf{R}}_{ji}} \cos \theta_{\hat{\mathbf{R}}_{ji}, \hat{\mathbf{k}}}}{\sin \theta_{\hat{\mathbf{e}}, \hat{\mathbf{R}}_{ji}} \sin \theta_{\hat{\mathbf{R}}_{ji}, \hat{\mathbf{k}}}}, \quad (\text{B11}) \\
f^{(0)}(\mathbf{k}, \mathbf{R}) &= \sum_{l=0}^{\infty} (2l+1) T_l(k) P_l(\hat{\mathbf{k}} \cdot \hat{\mathbf{R}}) \\
&\quad \times \left(c_l(kR) - \frac{c_l(kR)}{ikR} + \frac{1}{i} \frac{dc_l(kR)}{d(kR)} \right), \quad (\text{B12}) \\
f^{(1)}(\mathbf{k}, \mathbf{R}) &= \sum_{l=1}^{\infty} (2l+1) T_l(k) P_l^1(\hat{\mathbf{k}} \cdot \hat{\mathbf{R}}) \frac{c_l(kR)}{ikR}. \quad (\text{B13})
\end{aligned}$$

Where $\theta_{\hat{\mathbf{r}}, \hat{\mathbf{r}'}} = \arccos(\hat{\mathbf{r}} \cdot \hat{\mathbf{r}'})$ and $\phi_{\hat{\mathbf{e}}, \hat{\mathbf{R}}_{ji}, \hat{\mathbf{k}}}$ is the dihedral angle between the plane containing $\hat{\mathbf{e}}$ and $\hat{\mathbf{R}}_{ji}$ and the plane containing $\hat{\mathbf{R}}_{ji}$ and $\hat{\mathbf{k}}$. P_l and P_l^1 are Legendre function and Associated Legendre polynomials, respectively. [52]

The analytical expressions within Plane Wave approximation are obtained by neglecting the second term of the single scattering wave $S_{i \rightarrow j}$ in Eq. (27) and replacing the modified scattering amplitude as follows:

$$\begin{aligned}
S_{i \rightarrow j}(\mathbf{k}, \mathbf{R}_{ji}) &\xrightarrow{\substack{\text{Plane Wave} \\ \text{approximation}}} \\
&\hat{\mathbf{e}} \cdot \hat{\mathbf{R}}_{ji} \mathcal{G}(k, R_{ji}) f(k, \theta_{\hat{\mathbf{R}}_{ji}, \hat{\mathbf{k}}}) e^{i\mathbf{k}\cdot\mathbf{R}_{iO}}, \quad (\text{B14})
\end{aligned}$$

where

$$f(k, \theta_{\hat{\mathbf{R}}_{ji}, \hat{\mathbf{k}}}) = \sum_{l=0}^{\infty} (2l+1) T_l(k) P_l(\hat{\mathbf{k}} \cdot \hat{\mathbf{R}}_{ji}), \quad (\text{B15})$$

is the ordinary scattering amplitude with spherical symmetry potential.

-
- [1] F. Krausz and M. Ivanov, Reviews of Modern Physics **81**, 163-234 (2009).
[2] M. Nisoli, P. Decleva, F. Calegari, A. Palacios, and F. Martín, Chemical Reviews **117**, 10760-10825 (2017).
[3] R. Borrego-Varillas, M. Lucchini, and M. Nisoli, Reports on Progress in Physics **85**, 066401 (2022).
[4] G. S. Rinehart (2023).
[5] M. Y. Amusia and L. V. Chernysheva, JETP Letters **112**, 673-679 (2020).
[6] J. Liang, M. Han, Y. Liao, J.-b. Ji, C. S. Leung, W.-C. Jiang, K. Ueda, Y. Zhou, P. Lu, and H. J. Wörner,

Nature Photonics (2024).

- [7] M. Schultze, M. Fiess, N. Karpowicz, J. Gagnon, M. Korbman, M. Hofstetter, S. Neppl, A. L. Cavalieri, Y. Komninos, T. Mercouris, et al., Science **328**, 1658 (2010).
[8] J. Vos, L. Cattaneo, S. Patchkovskii, T. Zimmermann, C. Cirelli, M. Lucchini, A. Kheifets, A. S. Landsman, and U. Keller, Science **360**, 1326 (2018).
[9] X. Gong, W. Jiang, J. Tong, J. Qiang, P. Lu, H. Ni, R. Lucchese, K. Ueda, and J. Wu, Physical Review X **12**, 011002 (2022).

- [10] M. Kotur, D. Guénot, A. Jiménez-Galán, D. Kroon, E. W. Larsen, M. Louisy, S. Bengtsson, M. Miranda, J. Mauritsson, C. L. Arnold, et al., *Nature Communications* **7** (2016).
- [11] V. Gruson, L. Barreau, A. Jiménez-Galan, F. Risoud, J. Caillat, A. Maquet, B. Carré, F. Lepetit, J.-F. Hergott, T. Ruchon, et al., *Science* **354**, 734-738 (2016).
- [12] A. Kaldun, A. Blättermann, V. Stooß, S. Donsa, H. Wei, R. Pazourek, S. Nagele, C. Ott, C. D. Lin, J. Burgdörfer, et al., *Science* **354**, 738-741 (2016).
- [13] M. Huppert, I. Jordan, D. Baykusheva, A. von Conta, and H. J. Wörner, *Physical Review Letters* **117**, 093001 (2016).
- [14] C. Cirelli, C. Marante, S. Heuser, C. L. M. Petersson, A. J. Galán, L. Argenti, S. Zhong, D. Busto, M. Isinger, S. Nandi, et al., *Nature Communications* **9** (2018).
- [15] V. Lorient, A. Marciniak, S. Nandi, G. Karras, M. Hervé, E. Constant, E. Plésiat, A. Palacios, F. Martín, and F. Lépine, *Journal of Physics: Photonics* **2**, 024003 (2020).
- [16] S. Nandi, E. Plésiat, S. Zhong, A. Palacios, D. Busto, M. Isinger, L. Neoričić, C. L. Arnold, R. J. Squibb, R. Feifel, et al., *Science Advances* **6**, eaba7762 (2020).
- [17] S. Heck, D. Baykusheva, M. Han, J.-B. Ji, C. Perry, X. Gong, and H. J. Wörner, *Science Advances* **7** (2021).
- [18] H. Ahmadi, E. Plésiat, M. Molioli, F. Frassetto, L. Polletto, P. Decleva, C. D. Schröter, T. Pfeifer, R. Moshhammer, A. Palacios, et al., *Nature Communications* **13** (2022).
- [19] X. Gong, S. Heck, D. Jelovina, C. Perry, K. Zinchenko, R. Lucchese, and H. J. Wörner, *Nature* **609**, 507-511 (2022).
- [20] M. Isinger, R. J. Squibb, D. Busto, S. Zhong, A. Harth, D. Kroon, S. Nandi, C. L. Arnold, M. Miranda, J. M. Dahlström, et al., *Science* **358**, 893-896 (2017).
- [21] D. Azoury, O. Kneller, S. Rozen, B. D. Bruner, A. Clergerie, Y. Mairesse, B. Fabre, B. Pons, N. Dudovich, and M. Krüger, *Nature Photonics* **13**, 54-59 (2018).
- [22] J. Peschel, D. Busto, M. Plach, M. Bertolino, M. Hofflund, S. Maclot, J. Vinbladh, H. Wikmark, F. Zapata, E. Lindroth, et al., *Nature Communications* **13** (2022).
- [23] S. Beaulieu, A. Comby, A. Clergerie, J. Caillat, D. Descamps, N. Dudovich, B. Fabre, R. Géneaux, F. Légaré, S. Petit, et al., *Science* **358**, 1288 (2017).
- [24] A. Kamalov, A. L. Wang, P. H. Bucksbaum, D. J. Haxton, and J. P. Cryan, *Physical Review A* **102**, 023118 (2020).
- [25] A. L. Cavalieri, N. Müller, T. Uphues, V. S. Yakovlev, A. Baltuška, B. Horvath, B. Schmidt, L. Blümel, R. Holzwarth, S. Hendel, et al., *Nature* **449**, 1029-1032 (2007).
- [26] I. Jordan, M. Huppert, D. Rattenbacher, M. Peper, D. Jelovina, C. Perry, A. von Conta, A. Schild, and H. J. Wörner, *Science* **369**, 974-979 (2020).
- [27] I. A. Ivanov, A. S. Kheifets, and V. V. Serov, *Physical Review A* **86**, 063422 (2012).
- [28] V. V. Serov, V. L. Derbov, and T. A. Sergeeva, *Physical Review A* **87**, 063414 (2013).
- [29] A. Chacon, M. Lein, and C. Ruiz, *Physical Review A* **89**, 053427 (2014).
- [30] P. Hockett, E. Frumker, D. M. Villeneuve, and P. B. Corkum, *Journal of Physics B: Atomic, Molecular and Optical Physics* **49**, 095602 (2016).
- [31] D. Baykusheva and H. J. Wörner, *The Journal of Chemical Physics* **146**, 124306 (2017).
- [32] V. V. Serov and A. S. Kheifets, *The Journal of Chemical Physics* **147** (2017).
- [33] S. Biswas, B. Förg, L. Ortmann, J. Schötz, W. Schweinberger, T. Zimmermann, L. Pi, D. Baykusheva, H. A. Masood, I. Lontos, et al., *Nature Physics* **16**, 778 (2020).
- [34] F. Ota, K. Yamazaki, D. Sébilleau, K. Ueda, and K. Hatada, *Journal of Physics B: Atomic, Molecular and Optical Physics* **54**, 024003 (2021).
- [35] L. Nagy, S. Borbély, and K. Póra, *Physics Letters A* **327**, 481-489 (2004).
- [36] X.-J. Liu, N. A. Cherepkov, S. K. Semenov, V. Kimberg, F. Gel'mukhanov, G. Prümper, T. Lischke, T. Tanaka, M. Hoshino, H. Tanaka, et al., *Journal of Physics B: Atomic, Molecular and Optical Physics* **39**, 4801-4817 (2006).
- [37] D. Akoury, K. Kreidi, T. Jahnke, T. Weber, A. Staudte, M. Schöffler, N. Neumann, J. Titze, L. P. H. Schmidt, A. Czasch, et al., *Science* **318**, 949-952 (2007).
- [38] N. Hara, K. Hatada, and C. R. Natoli, *Physical Review A* **106**, 052807 (2022).
- [39] H. D. Cohen and U. Fano, *Physical Review* **150**, 30-33 (1966).
- [40] S. Heck, M. Han, D. Jelovina, J.-B. Ji, C. Perry, X. Gong, R. Lucchese, K. Ueda, and H. J. Wörner, *Physical Review Letters* **129**, 133002 (2022).
- [41] S. Grundmann, D. Trabert, K. Fehre, N. Strenger, A. Pier, L. Kaiser, M. Kircher, M. Weller, S. Eckart, L. P. H. Schmidt, et al., *Science* **370**, 339-341 (2020).
- [42] O. Hemmers, H. Wang, P. Focke, I. A. Sellin, D. W. Lindle, J. C. Arce, J. A. Sheehy, and P. W. Langhoff, *Physical Review Letters* **87**, 273003 (2001).
- [43] P. Langhoff, J. Arce, J. Sheehy, O. Hemmers, H. Wang, P. Focke, I. Sellin, and D. Lindle, *Journal of Electron Spectroscopy and Related Phenomena* **114-116**, 23-32 (2001).
- [44] I. A. Ivanov, A. S. Kheifets, and K. T. Kim, *Scientific Reports* **11** (2021).
- [45] H. A. Bethe and E. E. Salpeter, *Quantum mechanics of one-and two-electron atoms* (Springer Science & Business Media, 2012).
- [46] I. Vela-Peréz, F. Ota, A. Mhamdi, Y. Tamura, J. Rist, N. Melzer, S. Uerken, G. Nalin, N. Anders, D. You, et al., *Physical Chemistry Chemical Physics* **25**, 13784-13791 (2023).
- [47] Y. Tamura, K. Yamazaki, K. Ueda, and K. Hatada, *Journal of Physics B: Atomic, Molecular and Optical Physics* **55**, 10LT01 (2022).
- [48] D. Dill and J. L. Dehmer, *The Journal of Chemical Physics* **61**, 692-699 (1974).
- [49] J. R. Taylor, *Scattering theory: the quantum theory of nonrelativistic collisions* (Courier Corporation, 2006), p.32.
- [50] D. V. Rezvan, K. Klysssek, S. Grundmann, A. Pier, N. M. Novikovskiy, N. Strenger, D. Tsitsonis, M. Kircher, I. Vela-Peréz, K. Fehre, et al., *Physical Review Letters* **129**, 253201 (2022).
- [51] U. Hergenhahn, O. Kugeler, A. Rüdél, E. E. Rennie, and A. M. Bradshaw, *The Journal of Physical Chemistry A* **105**, 5704-5708 (2001).
- [52] J. M. de Leon, J. J. Rehr, C. R. Natoli, C. S. Fadley, and J. Osterwalder, *Physical Review B* **39**, 5632 (1989).
- [53] D. Sébilleau, C. Natoli, G. M. Gavaza, H. Zhao, F. Da Pieve, and K. Hatada, *Computer Physics Com-*

munications **182**, 2567 (2011).

[54] J. J. Rehr and R. C. Albers, *Physical Review B* **41**, 8139-8149 (1990).